View Article Online
View Journal

Dalton Transactions

An international journal of inorganic chemistry

Accepted Manuscript

This article can be cited before page numbers have been issued, to do this please use: D. Bellotti, M. Rowinska-Zyrek and M. Remelli, *Dalton Trans.*, 2020, DOI: 10.1039/D0DT01626H.

ROYAL SOCIETY OF CHEMISTRY

rsc.li/dalton

View Article Online
DOI: 10.1039/D0DT01626H

ARTICLE

Novel insights into the metal binding ability of ZinT periplasmic protein from *Escherichia coli* and *Salmonella enterica*

Received 00th January 20xx,
Accepted 00th January 20xx

DOI: 10.1039/x0xx00000x

Denise Bellotti,[a,b] Magdalena Rowińska-Żyrek[b] and Maurizio Remelli*[a]

ZinT mediated Zn(II) uptake is one of the major differences in the metabolism of human and bacterial cells that can be challenged when looking for possible highly selective metal-based therapeutics. ZinT is a 216-amino acid periplasmic protein expressed by Gram-negative bacteria, which shuttles Zn(II) ions to the ZnuABC transporter under zinc-limiting conditions. The suggested metal-binding sites of ZinT correspond to a domain containing three highly conserved histidine residues (His 167, 176 and 178) and to the N-terminal histidine-rich loop HGHHXH (residues 24–29). The coordination chemistry of ZinT complexes with Zn(II) and Cu(II) has been investigated. The present work is focused on the protected peptides Ac-^{24}HGHHSH^{29}-NH_2 and Ac-^{166}DHIIAPRKSSHFH^{178}-NH_2 as models for the putative metal binding sites of ZinT from *Escherichia coli* (*Ec*ZinT), and Ac-^{24}HGHHAH^{29}-NH_2 and Ac-^{166}DHIIAPRKSAHFH^{178}-NH_2 from the ZinT protein expressed by *Salmonella enterica* sv. Typhimurium (*Se*ZinT). The investigated peptides are able to form stable mono-nuclear complexes where the histidine residues represent the principal metal anchoring sites. ZnuA (a periplasmic component of the ZnuABC transporter) metal binding site exhibits a higher affinity for Zn(II) than ZinT, suggesting that the two proteins interaction through the formation of a binary complex may involve the metal transfer from ZinT to ZnuA. On the contrary, this would not occur for Cu(II), since ZinT complexes are more stable. Furthermore, at acidic pH, where the antimicrobial peptide calcitermin is biologically active, it also binds the metal ions with higher affinity than ZinT, representing a possible efficient competitor and antagonist of ZinT in the host human organism.

Introduction

The dramatic dissemination of antibiotic-resistant microorganisms represents both a serious threat and a scientific challenge of the modern age. The acquisition of metals from the host environment is a fundamental aspect of infections and deeper insights into the mechanism of metal trafficking in pathogens can provide crucial information to design new effective antimicrobial treatments.[1-3] Several pathogenic microorganisms are capable of expressing metallophore systems for the purpose to sequester metals from the host environment. In the process of nutritional immunity, in fact, the host and the pathogen compete for the acquisition of metallic nutrients and, therefore, the relative metal binding affinity and the specific coordination properties can seriously affect the activity and the effectiveness of the involved systems.[4-7]

The Zn(II) assimilation pathway provided by the ZinT/ZnuABC transport system is a promising target to develop novel treatments against infectious diseases, since this metal transporter does not have homologues in eukaryotic cells and it can therefore assure high specificity and selectivity, minimizing collateral side effects on patients.[8] The high-affinity Zn(II) uptake system ZnuABC belongs to the family of ATP-binding cassette transporters and it is composed of three proteins: ZnuA (periplasmic metallochaperone), ZnuB (membrane permease) and ZnuC (ATPase component).[9, 10] Recent studies have also identified an additional auxiliary periplasmic component of bacterial ZnuABC system, which collaborates with ZnuA in the mechanism of Zn(II) recruitment from the periplasmic environment under severe zinc-limited conditions. This protein is known as ZinT (formerly named YodA) and it is expressed by many Gram-negative bacteria, including *Escherichia coli* and *Salmonella enterica*.[11-14] Interestingly, recent studies have also demonstrated that ZinT and ZnuA can specifically interact together to form a binary system, but only if they are in a Zn(II)-bound form.[8, 14, 15]

An efficient metal ions import is doubtless critical for *Escherichia coli* and *Salmonella enterica* pathogenicity, together with a proficient resistance system that can prevent microbial cells from heavy metals poisoning. Interestingly, the physiological role of ZinT is related not only to Zn(II) homeostasis but also to cellular metal detoxification. In fact, beside zinc shortage, its expression can be upregulated upon cadmium stress, inducing the protein accumulation in the periplasmic region.[16] Furthermore, ZinT exhibits extremely versatile metal binding properties and affinity for several other divalent metal ions.[15, 17]

Various crystal structures of ZinT from *Escherichia coli* (*Ec*ZinT) and *Salmonella enterica* sv. Typhimurium (*Se*ZinT) have

[a] Department of Chemical and Pharmaceutical Sciences, University of Ferrara, Luigi Borsari 46, 44121 Ferrara, Italy.
[b] Faculty of Chemistry, University of Wrocław, F. Joliot-Curie 14, 50-383 Wroclaw, Poland.

† Electronic Supplementary Information (ESI) available. See DOI: 10.1039/x0xx00000x

been reported, including Zn(II), Ni(II) and Cd(II) complexes (Protein Data Bank (PDB) entries: 1OEJ, 1OEK, 1OEE, 5AQ6, 5YXC, 1S7D, 1TXL, 5XM5, 4AW8, 4AYH, 4ARH). According to ZinT evolutionarily highly conserved amino acid sequence and to its three-dimensional structures, the most probable identified metal-binding sites are two regions, corresponding to *(i)* the sequence containing the three histidine residues in position 167, 176 and 178,[18, 19] and *(ii)* the highly conserved histidine-rich loop (HGHHXH) located at the N-terminal portion of the protein.[8, 15, 20] No thermodynamic data are available for ZinT metal binding sites and the accepted evidence encouraged to proceed with the investigation of Zn(II) and Cu(II) complexes with ZinT in both *E. coli* (*Ec*ZinT) and *S. enterica* (*Se*ZinT) species. Although ZinT physiological role in Cu(II) metabolism has not been confirmed yet, Cu(II) is essential for many enzymatic processes and it can be extremely toxic for microbes, since it generates reactive oxygen species (ROS), increasing the cellular oxidative stress.[21, 22] On the contrary, Zn(II) is redox inactive and is crucial for pathogen subsistence, participating in many cellular reactions as coenzyme or cofactor.[23-25] Moreover, the importance of these ions in the process of nutritional immunity is decisive as well: human organism can rely on a variety of proteins and antimicrobial peptides in order to sequester Zn(II) and Cu(II) and induce pathogens starvation, interfering with their virulence and survival in the host organism.[26, 27]

The present paper describes a detailed study on Zn(II) and Cu(II) complexes with the following amino- and carboxyl-terminal protected peptides: Ac-HGHHSH-NH_2 (**L1**) and Ac-HGHHAH-NH_2 (**L2**), which serve as models of the N-terminal histidine-rich loop (24–29 amino acid sequence) of *Ec*ZinT and *Se*ZinT, respectively; and Ac-DHIIAPRKSSHFH-NH_2 from *Ec*ZinT (**L3**) and Ac-DHIIAPRKSAHFH-NH_2 from *Se*ZinT (**L4**), which correspond to the 166–178 amino acid sequence encompassing the three highly conserved His residues (see Figure 1). It is worth to emphasize the punctual Ser-to-Ala substitution occurring for each couple of peptide homologues **L1**/**L2** and **L3**/**L4**. Since small changes in the peptide primary structure can affect the metal binding behaviour, a deep investigation of the complex-formation equilibria is required to fully understand the coordination properties of *Ec*ZinT and *Se*ZinT and to highlight possible differences between the two bacterial species behaviour. The thermodynamic and spectroscopic analysis of metal-ZinT complexes has been performed by means of several experimental techniques. The complex formation equilibria have been investigated over a wide pH range through high-resolution mass spectrometry and potentiometric titrations. A complementary description of the metal coordination sphere and molecular geometry has been performed by UV-Vis spectrophotometry, circular dichroism (CD) and electronic paramagnetic resonance (EPR).

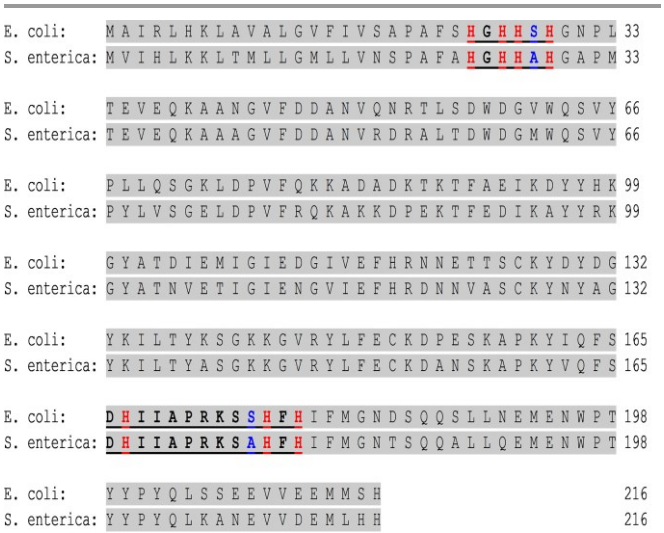

Figure 1. Protein sequence alignment between *Ec*ZinT and *Se*ZinT.[15, 20] Studied regions are marked in color.

Experimental

Materials

All peptides (Ac-HGHHSH-NH_2, Ac-HGHHAH-NH_2, Ac-DHIIAPRKSSHFH-NH_2 and Ac-DHIIAPRKSAHFH-NH_2) were purchased from KareBay Biochem (USA) with a certified purity of 98%. They were used as received. $Zn(ClO_4)_2 \cdot 6H_2O$ and $Cu(ClO_4)_2 \cdot 6H_2O$ were extra pure products (Sigma-Aldrich); the concentrations of their stock solutions were standardised by EDTA titration and periodically checked via ICP-MS. The carbonate-free stock solution of 0.1 mol dm^{-3} NaOH was purchased from Sigma-Aldrich and standardized with the primary standard potassium hydrogen phthalate (99.9% purity) by potentiometry. The $HClO_4$ stock solution was prepared by diluting concentrated $HClO_4$ (Sigma-Aldrich) and then standardizing with NaOH. The ionic strength was adjusted to 0.1 mol dm^{-3} by adding $NaClO_4$ (Sigma-Aldrich). Grade A glassware was employed throughout. All sample solutions were prepared with freshly doubly distilled water.

Potentiometric measurements

Stability constants for proton and metal complexes were calculated from pH-metric titration curves registered at T=298 K and ionic strength 0.1 mol dm^{-3} ($NaClO_4$) using a total volume of 3 cm^{-3}. The potentiometric apparatus consisted of a Metrohm 905 Titrando pH-meter system provided with a Metrohm LL Unitrode glass electrode and a dosing system 800 Dosino, equipped with a 2 ml micro burette. High purity grade argon was gently blown over the sample solution to ensure an inert atmosphere. Solutions were titrated under constant-speed magnetic stirring with 0.1 mol dm^{-3} carbonate-free NaOH. The electrode was daily calibrated for hydrogen ion concentration by titrating $HClO_4$ with standard NaOH under the same experimental conditions as above. The standard potential and the slope of the electrode couple were computed by means of the Glee[28] program. The purities and the exact concentrations of the ligand solutions were potentiometrically determined using the Gran method.[29] The HYPERQUAD[30] program was employed to calculate the overall formation constant (β), referring to the following equilibrium:

$pM+qL+rH \leftrightarrows M_pL_qH_r$

(charges omitted; p is 0 in the case of ligand protonation; r can be negative). Step formation constants (K) and/or acid dissociation constants (K_a) are also reported. The computed standard deviations (referring to random errors only) were given by the program itself and are shown in parentheses as uncertainties on the last significant figure. Hydrolysis constants for Cu(II) and Zn(II) ions were taken from the literature: $[CuH_{-1}]^+$ logβ = -7.7, $[Cu_2H_{-2}]^{2+}$ logβ = -10.75, $[Cu_3H_{-4}]^{2+}$ logβ = -21.36, $[CuH_{-4}]^{2-}$ logβ = -39.08;[31] $[ZnH_{-1}]^+$ logβ = -8.96, $[ZnH_{-2}]$ logβ = -16.9, $[ZnH_{-3}]^-$ logβ = -28.4, $[ZnH_{-4}]^{2-}$ logβ = -41.2.[32] The distribution diagrams were computed using the HYSS program.[33] A comparison of the overall metal binding ability of the different ligands were performed by computing the competition diagrams. They represent a simulation of a solution containing the metal and the two (or more) ligands (or *vice versa*) and are based on the previously obtained binary speciation models, admitting that all the components compete to form the respective binary complexes without mixed species formation. This is a reasonable approximation in the case of peptides, which most often form only 1:1 complexes where the peptide completely wraps the metal ion.

Mass spectrometric measurements

High-resolution mass spectra were obtained on a BrukerQ-FTMS spectrometer (Bruker Daltonik, Bremen, Germany), equipped with an Apollo II electrospray ionization source with an ion funnel. The mass spectrometer operated in the positive ion mode. The instrumental parameters were as follows: scan range m/z 100–2500, dry gas nitrogen, temperature 453 K and ion energy 5 eV. The capillary voltage was optimized to the highest signal-to-noise ratio, corresponding to 4500 V. The small changes in voltage (±500 V) did not significantly affect the optimized spectra. The samples (Zn(II):ligand and Cu(II):ligand in a 0.9:1 stoichiometry, $[ligand]_{tot}=0.5 \cdot 10^{-3}$ mol dm^{-3}) were prepared in a 1:1 methanol–water mixture at different pH values and were infused at a flow rate of 3 µL min^{-1}. The instrument was externally calibrated with a Tunemix™ mixture (Bruker Daltonik, Germany) in quadratic regression mode. Data were processed using the Bruker Compass DataAnalysis 3.4 program. The mass accuracy for the calibration was better than 5 ppm, enabling together with the true isotopic pattern (using SigmaFit) an unambiguous confirmation of the elemental composition of the obtained complex.

Spectroscopic measurements

The absorption spectra were recorded on a Varian Cary300 Bio spectrophotometer, in the range 200–800 nm, using a quartz cuvette with an optical path of 1 cm. Circular dichroism (CD) experiments were recorded on a Jasco J-1500 CD spectrometer at 298 K in a 0.01 cm and 1 cm quartz cells for the spectral ranges of 180–270 and 200–800 nm, respectively. The ligands were dissolved in a water solution containing $4 \cdot 10^{-3}$ mol dm^{-3} $HClO_4$ at 0.1 mol dm^{-3} $NaClO_4$. Ligand concentration was $0.5 \cdot 10^{-3}$ mol dm^{-3} (200–800 nm range) and $0.1 \cdot 10^{-3}$ mol dm^{-3} (180–270 nm range). Cu(II) to ligand molar ratio was 0.9:1. The UV-Vis and CD spectroscopic parameters were extracted from the spectra obtained at the pH values corresponding to the maximum concentration of each particular species, based on distribution diagrams. Electron paramagnetic resonance (EPR) spectra were recorded in liquid nitrogen on a Bruker ELEXSYS E500 CW-EPR spectrometer at X-band frequency (9.5 GHz) and equipped with an ER 036TM NMR teslameter and an E41 FC frequency counter. Ethylene glycol (30%) was used as a cryoprotectant. Ligand concentration was $1.0 \cdot 10^{-3}$ mol dm^{-3} and Cu(II) to ligand ratio = 0.9:1. The EPR parameters were analysed by simulating the experimental spectra using WIN-EPR SIMFONIA software, version 1.2 (Bruker).

Results and discussion

Ligand protonation

The investigated peptides are protected at their amino- and carboxyl-terminus by means of acetylation and amidation, respectively. The ligand acid-base behaviour, therefore, only depends on the amino acid side chain properties; the corresponding experimental overall and step protonation constants are reported in Table 1. The amidic groups of the peptide backbone are very weak acids (p$K_a \approx 15$)[34] and the spontaneous release of their protons cannot occur in the explored pH range (2.5 – 10.5). For each peptide, the obtained *macro*-constants reported in Table 1 have been compared with literature data in order to assign the protonation step to the corresponding functional group. The term L here indicates the ligand in its unprotonated form where all the dissociable protons have been released; the net charge of L is zero for all the investigated ligands. However, in the case of **L1** and **L2**, L corresponds to a peptide without any charged groups, while for **L3** and **L4** L is a zwitterionic species, due to the presence of the negatively charged carboxylate group of Asp residue and the positively charged arginyl guanidinium group, which is always protonated in the pH range here employed.

In ligands **L1** and **L2** there are four histidine residues which are involved in acid-base equilibria. The obtained pK_a values range from 5.73 to 7.38, in good agreement with the literature protonation constants for histidine residues.[35] Ligands **L3** and **L4** contain five functional groups with dissociable protons: the carboxylic side chain of aspartic acid, the imidazole groups of the three histidine residues and the lysyl amino group. In the case of both the ligands, we attribute the lowest pK_a to the carboxylic acid of the Asp residue (4.06 and 3.92), while the next three protonation steps can be assigned to the histidine residues with pK_as values ranging from 5.61 to a maximum of 6.91. The highest formation constants, 9.50 (**L3**) and 9.65 (**L4**), most likely correspond to the lysine ε-amino groups. These rather low pK_a values can be related to Lys proximity to the protonated arginyl guanidinium group. Indeed, comparable low pK_as (even lower than 9) for lysine deprotonation are found in literature, where the increased acidity is explained by the presence of vicinal positively charged side chains (Lys, Orn and Arg).[36-38] Notably, the Ser-to-Ala substitution does not

View Article Online DOI: 10.1039/D0DT01626H

Table 1. Overall (log β) and step (log K) protonation constants for all the investigated ligands (Ac-HGHHSH-NH_2 (**L1**), Ac-HGHHAH-NH_2 (**L2**), Ac-DHIIAPRKSSHFH-NH_2 (**L3**) and Ac-DHIIAPRKSAHFH-NH_2 (**L4**)) at T=298 K and I=0.1 mol dm^{-3} ($NaClO_4$). Values in parentheses are standard deviations on the last significant figure.

	L1		L2		L3		L4	
Species	**logβ**	**log$K$**	**logβ**	**log$K$**	**logβ**	**log$K$**	**logβ**	**log$K$**
HL^{+}	7.38(9)	7.38	7.16(9)	7.16	9.53(3)	9.53	9.65(2)	9.65
H_2L^{2+}	13.87(6)	6.50	13.75(5)	6.59	16.27(3)	6.74	16.56(4)	6.90
H_3L^{3+}	19.87(9)	6.00	19.68(8)	5.93	22.59(2)	6.32	22.91(3)	6.35
H_4L^{4+}	25.60(7)	5.73	25.46(6)	5.78	28.17(3)	5.58	28.64(3)	5.74
H_5L^{5+}					32.22(3)	4.06	32.56(4)	3.92

significantly affect the acid-base properties of the investigated peptides, since the obtained protonation constants of each homologues couple Ac-HGHHSH-NH_2/Ac-HGHHAH-NH_2 and Ac-DHIIAPRKSSHFH-NH_2/Ac-DHIIAPRKSAHFH-NH_2 are comparable.

Cu(II) complexes

High resolution mass spectra revealed the formation of mononuclear Cu(II) complexes under the employed experimental conditions. Signals corresponding to various sodium and potassium adducts, together with the differently protonated free ligand and metal complexes have been detected. No poly-nuclear complexes or bis-complexes have been identified. Mass spectra are reported in Figures S1–S4 ESI. The speciation models obtained by potentiometry confirm the occurrence in solution of 1:1 metal complexes, in accordance with the MS results. The complex-formation constants for Cu(II) are reported in Table 2, and the corresponding species distribution diagrams are shown in Figures 2, S5–S7 ESI. Spectroscopic data are summarised in Tables S1–S4 ESI and UV-Vis, CD and EPR spectra are depicted in Figures 3, 4 and S8–16 ESI.

Potentiometric measurements revealed that Cu(II) is able to interact with **L1** and **L2** starting from pH 3. The first identified species is $[CuH_2L]^{4+}$; the speciation diagrams plotted in Figures 2 and S5 ESI show that its percentage of formation in solution remains rather low (25%) since this complex is quickly substituted the $[CuHL]^{3+}$ species, that is by far the most abundant complex in solution from pH 4.5 until pH 6. In $[CuH_2L]^{4+}$ the ligand has already lost two acidic protons from its fully protonated histidine residues which can thus bind the metal ion and form a ($2N_{Im}$) species. The following deprotonation step, associated to the formation of $[CuHL]^{3+}$ complex, has a pK_a value of 4.45 (**L1**) or 4.46 (**L2**), both attributable to the deprotonation and binding of a third imidazole group. This step is also accompanied by a shift of the visible absorption spectra towards shorter wavelengths, thus indicating an increase of the number of coordinated nitrogen atoms around the Cu(II) (Figures 3 and S9 ESI). The measured λ_{max} values for the complex solutions at pH ≈ 5.5 – where $[CuHL]^{3+}$ is the most abundant species – are 637 nm for Cu(II)-**L1** and 626 nm for Cu(II)-**L2**, and suggest a ($3N_{Im}$) coordination for both the systems. The next deprotonation step occurs with a pK_a = 6.26 (**L1**) and 6.37 (**L2**), leading to the species $[CuL]^{2+}$. In this case the most reasonable hypothesis is the release of the proton from an amide group of the peptide backbone, which can be ionized thank to the interaction with the Cu(II) ion. In fact, the corresponding *d–d* band of UV-Vis spectra at pH around 6.5–7, where $[CuL]^{2+}$ reaches its maximum of formation (Figures 2 and S5 ESI), is characterized by λ_{max} value (**L1**: 608 nm and **L2**: 600 nm) very close to the expected absorption wavelength for a ($2N_{Im}$, N^{-}) complex (604 nm[34]); the fourth equatorial position should be occupied by a water molecule. Therefore, in the formation of $[CuL]^{2+}$ species, a N-amide should substitute one histidine residue in the equatorial plane of the metal coordination sphere. Moreover, starting from pH 6, a slight variation of the CD spectra likely confirms the Cu(II) interaction with the backbone N-amide (Figures 4 and S10 ESI). EPR parameters at pH 6.5 also indicate a prevalence of a 3N coordination (**L1**: $g_{//}$ = 2.25, $A_{//}$ = 180.4; **L2**: $g_{//}$ = 2.22, $A_{//}$ = 175.3).[39] Increasing the pH value, the species $[CuH_{-1}L]^{+}$ and $[CuH_{-2}L]$ are formed with the following corresponding acid

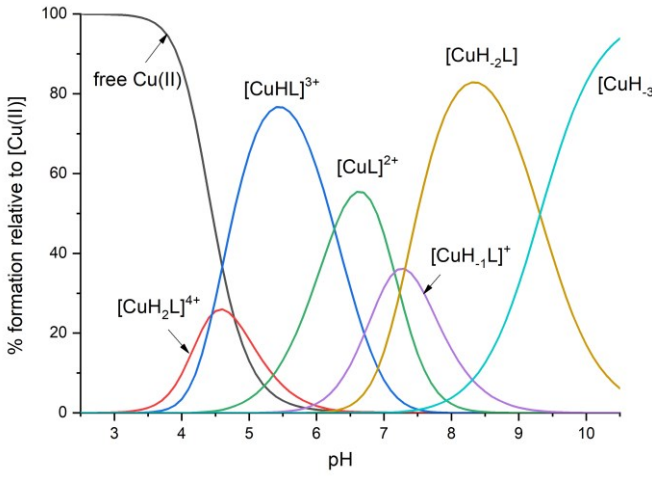

Figure 2. Species distribution diagram relative to Cu(II)/**L1** complexes; M:L molar ratio = 0.9:1; $C_{Cu(II)} = 0.45 \cdot 10^{-3}$ mol dm^{-3}.

View Article Online
DOI: 10.1039/D0DT01626H

Table 2. Overall stability constants (log β) and acid dissociation constants (pK_a) of Cu(II) complexes with all the investigated ligands (Ac-HGHHSH-NH_2 (**L1**), Ac-HGHHAH-NH_2 (**L2**), Ac-DHIIAPRKSSHFH-NH_2 (**L3**) and Ac-DHIIAPRKSAHFH-NH_2 (**L4**)) at T=298 K and I=0.1 mol dm^{-3} ($NaClO_4$). Values in parentheses are standard deviations on the last significant figure.

	L1		L2		L3		L4	
Species	**logβ**	**pK_a**	**logβ**	**pK_a**	**logβ**	**pK_a**	**logβ**	**pK_a**
$[CuH_2L]^{4+}$	19.72(8)	4.45	19.4(1)	4.46	22.26(3)	5.32	22.53(4)	5.40
$[CuHL]^{3+}$	15.27(3)	6.26	14.93(4)	6.37	16.94(4)	5.74	17.13(5)	5.68
$[CuL]^{2+}$	9.00(7)	7.15	8.56(8)	7.24	11.19(4)	6.19	11.45(5)	6.35
$[CuH_{-1}L]^{+}$	1.85(8)	7.31	1.32(9)	7.38	5.00(4)	9.03	5.10(4)	9.65
$[CuH_{-2}L]$	-5.46(7)	9.31	-6.06(8)	9.52	-4.03(7)	10.18	-4.54(6)	10.35
$[CuH_{-3}L]^{-}$	-14.78(8)		-15.59(9)		-14.20(7)		-14.90(5)	

dissociation constants: pK_as = 7.15 and 7.31 (**L1**) and pK_as = 7.24 and 7.38 (**L2**). From pH 6.5 to pH 9, the absorption spectra of both the systems undergo a further blue-shift towards wavelengths of maximum absorption around 560 nm, suggesting the binding of one additional nitrogen atom, most likely in substitution of the water molecule. An unequivocal description of the coordination mode of each formed complex in this pH range is not possible. However, one deprotonation step can be attributed to the mere release of the proton from the last protonated histidine, without directly participating to the metal complexation – the corresponding step constants (7.31 for **L1** and 7.24 for **L2**) are in fact very close to those measured in the absence of metal ion. The other step can be ascribed to the release of the acidic proton from a second backbone amide, which binds Cu(II) in equatorial position, finally obtaining a ($2N_{Im}$, $2N^-$) coordination. The 4N binding mode for $[CuH_{-2}L]$ is also confirmed by EPR results.[39] Moreover, the increased signal intensity of CD spectra in the above considered pH range is consistent with the increase of N-amides donors. Finally, at pH > 9, the last complex $[CuH_{-3}L]^-$ can be detected, characterized by a pK_a = 9.31 (**L1**) or pK_a = 9.52 (**L2**). The visible spectra in the most alkaline pH range suggest the coordination of a third N-amide in the equatorial plane of the complex, in substitution of an imidazole. The formation of the $[CuH_{-3}L]^-$ specie causes a clear blue-shift of the Vis-absorption band to λ_{max} = 523 nm, in the case of Cu(II)-**L1** system, and 540 nm for Cu(II)-**L2**. While the former wavelength value perfectly agrees with the expected literature value (522 nm) for a (N_{Im}, $3N^-$) coordination mode, the latter value suggests the presence of an axial donor group, most likely a further histidine, which is known to induce a red-shift. An exhaustive explanation of this different behaviour is not simple: it can be suggested that, in **L2**, the additional coordination of an axial imidazole is (possibly electrostatically) hindered by the serine residue of **L1**.

In the case of **L3** and **L4**, Cu(II) complexes begin to form at pH 3.5. Under such acidic conditions, the metal coordination can involve the carboxylate side chain of Asp and the histidine residues. The stoichiometry of the first detected complex $[CuH_2L]^{4+}$ suggests that two histidine residue and the carboxylic acid are already deprotonated. At such acidic pH the binding of the two imidazole groups likely occurs, while the coordination of COO^- is questionable. However, by subtracting the logβ_{012} to the logβ_{112} for each ligand, i.e. the contribution of the still protonated groups, one obtains 5.85 (**L1**), 5.65 (**L2**), 5.99 (**L3**) and 5.97 (**L4**). The latter two values are slightly higher than the former ones, supporting the hypothesis of the additional carboxylate coordination, in agreement with spectroscopic results. UV-Vis spectra recorded at pH 5 (Figures S12 and S15 ESI), where $[CuH_2L]^{4+}$ reaches its maximum of formation in solution, show a *d–d* band centred at λ= 654 nm (Cu(II)-**L3**) and 650 nm (Cu(II)-**L4**), which is in reasonably good agreement with the literature data for a ($2N_{Im}$, COO^-) Cu(II) complex (λ= 663 nm).[34] The binding groups most likely occupy three equatorial positions of the metal coordination sphere in a distorted octahedral geometry. The obtained $g_{//}$ and $A_{//}$ values of EPR spectra recorded at pH 5.3 (Figures S14, S17 and Tables S3, S4 ESI) also confirm a (2N, O) coordination. The $[CuH_2L]^{4+}$ species loses a further proton with pK_a = 5.32 (**L3**) or 5.40 (**L4**), as the result of the deprotonation of the third histidine residue which can coordinate the metal ion in the fourth equatorial position. This hypothesis is supported by the fact that the expected wavelength of maximum absorption for a ($3N_{Im}$, COO^-) complex is 607 nm and the experimentally obtained λ_{max} values for $[CuHL]^{3+}$ are 603 nm and 610 nm for **L3** and **L4**, respectively. Increasing the pH value, two further deprotonation steps give rise to $[CuL]^{2+}$ and $[CuH_{-1}L]^+$. The corresponding pK_a values (see Table 2) agree with the hypothesis of the Cu(II)-induced ionization of two backbone amides. The metal interaction with the peptide backbone usually produces a stronger CD absorption, due to the proximity of the N-amide donor group to the peptide chiral centres, and the CD spectra in Figures S13 and S16 ESI do not show a remarkable CD activity until pH = 6, i.e. when $[CuL]^{2+}$ and $[CuH_{-1}L]^+$ complexes become the predominant species in solution. According to the UV-Vis absorption spectra and EPR data, the formed complexes likely involve 4 N equatorial donor groups, with a ($3N_{Im}$, N^-) and ($2N_{Im}$, $2N^-$) coordination mode for $[CuL]^{2+}$ and $[CuH_{-1}L]^+$, respectively. The next deprotonation step leads to the formation of $[CuH_{-2}L]$ complex. The proton release occurs with pK_a = 9.03 for **L3** and pK_a = 9.65 for **L4** and it is reasonably attributable to the lysine ε-

View Article Online
DOI: 10.1039/D0DT01626H

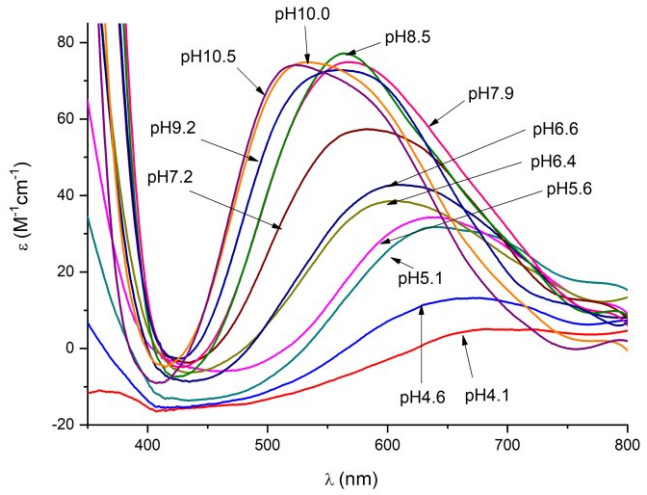

Figure 3. Vis absorption spectra for Cu(II) complexes with **L1**; M:L ratio = 0.9:1. $C_{Cu(II)}$ = 0.45 · 10^{-3} mol dm^{-3}; optical path 1 cm.

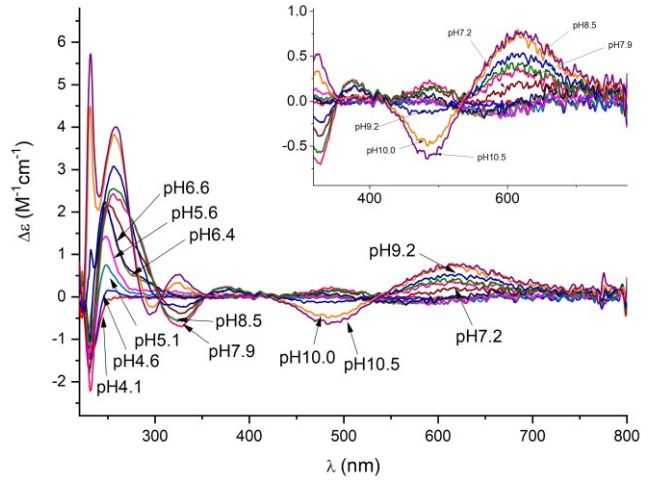

Figure 4. CD spectra for Cu(II) complexes with **L1**; M:L ratio = 0.9:1. $C_{Cu(II)}$ = 0.45 · 10^{-3} mol dm^{-3}; optical path 1 cm.

amino group. In the case of **L3** the recorded UV-Vis spectra for $[CuH_{-2}L]$ (pH ≈ 10) show a red-shift towards λ_{max} = 544 nm, suggesting a variation in the Cu(II) coordination environment. The slight changes of the EPR parameters (Figure S14 ESI) also suggest an apical perturbation in the Cu(II) coordination sphere, due to the possible interaction with the lysine ε-NH_2 moiety. On the contrary, in the case of **L4** no spectroscopic changes are observed. The dissociation constant of 9.65 is also in perfect agreement with the hypothesis of the lysine deprotonation without being involved in the metal complexation (pK_a = 9.65 in the free ligand). Lastly, under the most alkaline conditions, the release of a further proton occurs with pK_a = 10.18 (**L3**) and 10.35 (**L4**), most likely corresponding to the deprotonation of the pyrrole-type nitrogen of a coordinated histidine.[40, 41] This hypothesis is supported by the absence of spectroscopic changes during the formation of $[CuH_{-3}L]^-$ complex, thus excluding the coordination of a third amidic nitrogen.

Zinc complex

The investigated systems are able to form Zn(II) complexes in a stoichiometric ratio 1:1 under the employed experimental conditions. Electrospray ionization mass spectra confirm the presence of only mononuclear species at different protonation degrees with all the studied systems. The most intense signals correspond to the free ligands and to their adducts with sodium and potassium ions; nevertheless, it was also possible to detect various Zn(II) complexes, confirming the speciation model obtained from potentiometric data. The corresponding *m/z* values and the superimposition of experimental and simulated isotopic patterns for the most intense Zn(II) complexes are shown in Figures S18–S21 ESI. Potentiometric calculations have been performed until pH 8, due to the formation of a precipitate at alkaline pH. The complex-formation constants are shown in Table 3 and the species distribution diagrams are plotted in Figures 5 and S22–S24 ESI.

In the case of Ac-HGHHSH-NH_2 (**L1**) and Ac-HGHHAH-NH_2 (**L2**), at the most acidic pH values, the free metal ion is prevailing and Zn(II) complexes begin to form only above pH 4.5–5 (Figures 5, S22 ESI). The di-protonated complex $[ZnH_2L]^{4+}$ is the first detected species for **L2**-Zn(II) system. Notably, its formation is not detectable in the case of **L1**, where the first identified species is instead $[ZnHL]^{3+}$. Most likely, the **L1** di-protonated complex is only a transient species, which cannot be detected by potentiometry due its low percentage of formation in solution. In the $[ZnH_2L]^{4+}$ complex two histidine residues should be already deprotonated and bound to the metal ion; the likely complex geometry is tetrahedral, where two water molecules complete the Zn(II) coordination sphere. The stoichiometry of the $[ZnHL]^{3+}$ complex for both systems suggests that Zn(II) coordination occurs by means of three imidazole groups ($3N_{Im}$). In the case of **L2** – where it has been possible to calculate the corresponding step dissociation constant – the pK_a value of 5.78 agrees with the hypothesis of deprotonation and coordination of a third His residue to form $[ZnHL]^{3+}$. Tetrahedral complex geometry most likely occurs also for this species, where the fourth donor group is a water molecule. Increasing the pH value, two further complexes are formed, $[ZnL]^{2+}$ and $[ZnH_{-1}L]^+$. The former species most likely derives from the $[ZnHL]^{3+}$ complex through the simple release of a proton from the coordinated water molecule; in the latter, the binding of a fourth histidine possibly takes place. Once again, the preferred Zn(II) tetrahedral geometry should be retained in $[ZnL]^{2+}$ with the formation of the mono-hydroxo complex ($3N_{Im}$, O^-). The coordination of the fourth histidine in $[ZnH_{-1}L]^+$ would instead lead to the formation of a pentacoordinate system ($4N_{Im}$, O^-) with a distorted pyramidal arrangement, which is not surprising considering the conformational flexibility of Zn(II) ion.[42, 43] A mix of tetrahedral and pyramidal species can also be hypothesized.

With the ligands Ac-DHIIAPRKSSHFH-NH_2 (**L3**) and Ac-DHIIAPRKSAHFH-NH_2 (**L4**), Zn(II) complexation begins at pH 4.5 with the formation of $[ZnH_2L]^{4+}$ and $[ZnHL]^{3+}$, although the

View Article Online
DOI: 10.1039/D0DT01626H

Table 3. Overall stability constants (log β) and acid dissociation constants (pK_a) of Zn(II) complexes with all the investigated ligands (Ac-HGHHSH-NH_2 (**L1**), Ac-HGHHAH-NH_2 (**L2**), Ac-DHIIAPRKSSHFH-NH_2 (**L3**) and Ac-DHIIAPRKSAHFH-NH_2 (**L4**)) at T=298 K and I=0.1 mol dm^{-3} ($NaClO_4$). Values in parentheses are standard deviations on the last significant figure.

	L1		L2		L3		L4	
Species	**logβ**	**pK_a**	**logβ**	**pK_a**	**logβ**	**pK_a**	**logβ**	**pK_a**
$[ZnH_2L]^{4+}$	-	-	17.3(1)	5.78	20.04(7)	6.28	20.17(5)	6.47
$[ZnHL]^{3+}$	11.85(7)	6.4	11.5(1)	6.0	13.76(5)	6.51	13.70(5)	6.61
$[ZnL]^{2+}$	5.5(1)	6.3	5.5(1)	6.1	7.25(3)	-	7.09(2)	-
$[ZnH_{-1}L]^{+}$	-0.82(7)	-	-0.57(3)	-	-	-	-	-

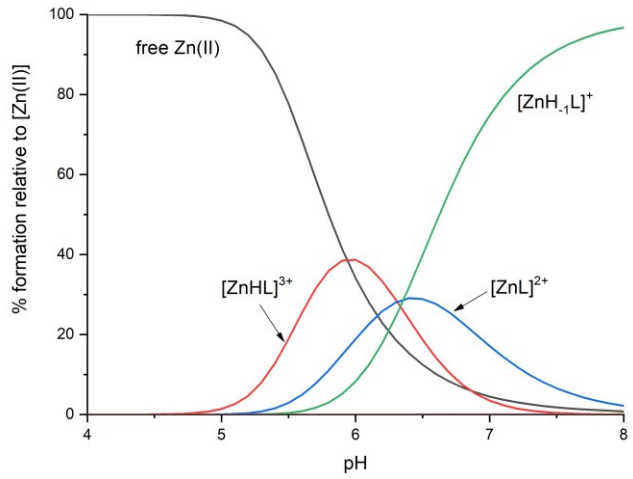

Figure 5. Species distribution diagram relative to Zn(II)/**L1** complexes; M:L molar ratio = 0.9:1; $C_{Zn(II)} = 0.45 \cdot 10^{-3}$ mol dm^{-3}.

solution remains dominated by the presence of free Zn(II) until pH about 6.5 (Figures S23, S24 ESI). In the first identified species $[ZnH_2L]^{4+}$, the proposed coordination hypothesis is ($2N_{Im}$, COO^-), where two histidine residues and the Asp carboxylic side chain are bound to Zn(II) and occupy three coordination positions of a tetrahedral conformation. The fourth donor group should be a water molecule. The $[ZnHL]^{3+}$ complex begins to form around pH 5–5.5. The related acid dissociation constants (**L3**: pK_a = 6.28; **L4**: pK_a = 6.47) suggest the coordination of the third His residue, which likely substitutes the carboxylate donor group in the metal coordination sphere to obtain a ($3N_{Im}$) binding mode. The third formed complex $[ZnL]^{2+}$ becomes the most abundant species above neutral pH in both the systems. According to its stoichiometry and the corresponding pK_a values, the ionization of the coordinated water molecule probably takes place and a ($3N_{Im}$, O^-) tetrahedral complex is obtained. Indeed, the relatively low pK_a values are not compatible with the hypothesis of lysine deprotonation in the explored pH range, since its ε-amino group dissociates at higher pH values (pK_a = 9.50 (**L3**) and 9.65 (**L4**) in the free ligands).

ZinT complex stability: pointing out the most effective metal binding site

In order to better evaluate and compare the coordination ability of the investigated systems, some competition plots have been drawn. They represent a simulation of solutions containing equimolar concentrations of the metal and the chosen ligands, admitting that all the peptides compete for the metal recruitment and that they form only the binary complexes described in the speciation models reported above.

It is important to stress out that the investigated model peptides belong to ZinT proteins of different pathogenic organisms, i.e. *E. coli* and *S. enterica*. The sequences are very similar in the two bacteria, but in the case of *S. enterica*, two serine residues (position 28 and 175 of ZinT protein sequence) are substituted by alanines. There are no explanations for such substitution in terms of ZinT biological role or virulence efficacy. Nevertheless, it is quite interesting to notice that this variation occurs in both the metal binding domains of ZinT. The competition diagrams plotted in Figures S25 and S26 ESI show the effects of Ser-to-Ala substitution on Cu(II) and Zn(II) complex stability. Although serine residues are not coordinated to the metal ion, their presence seems to contribute to the overall stability of Cu(II) systems when deprotonation of backbone amides occurs, as already previously observed for similar systems.[44] This effect is particularly evident in the case of **L1** and **L2**, where the lack of serine in the sequence causes a drop of metal affinity around pH 6 (Figure S25a ESI). Cu(II) complexes with **L3** (*E. coli* fragment) are also more stable than Cu(II)-**L4** systems; however, here the difference is lower (Figure S25b ESI), possibly due to the presence of an additional serine residue in the sequence which reduces the effect of Ser-to-Ala substitution. It is worth to note that the higher Cu(II) affinity for **L3** is consistent with the hypothesis of the metal interaction with an apical lysine (see above), which contributes to stabilize the complex by wrapping the metal centre. In the case of Zn(II) complexes (Figure S26 ESI), where amides are not involved in the coordination, the contribution of the serine residue on complexation does not have a clear and definite trend; the behaviour of the two binding sites is different although the binding modes are quite similar. A deeper investigation would be required to completely clarify these features.

An overall comparison among the four systems gives some clues about the biological role of the two identified metal

View Article Online DOI: 10.1039/D0DT01626H

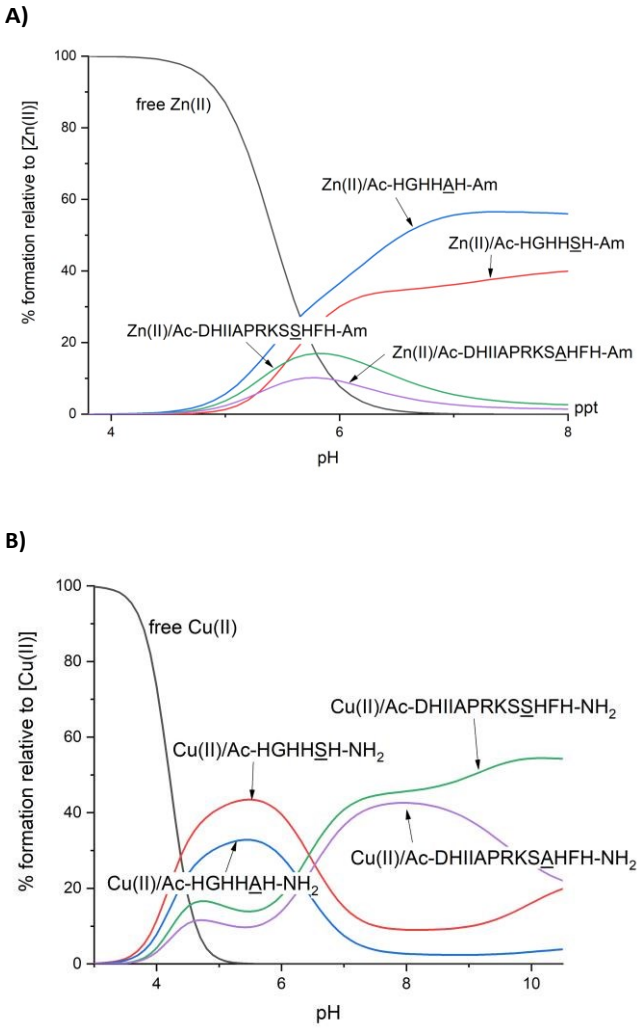

Figure 6. Competition plots for a solution containing equimolar concentration ($1 \cdot 10^{-3}$ mol dm^{-3}) of metal ion, **L1** = Ac-HGHHSH-NH_2, **L2** = Ac-HGHHAH-NH_2, **L3** = Ac-DHIIAPRKSSHFH-NH_2 and **L4** = Ac-DHIIAPRKSAHFH-NH_2. A) Zn(II), B) Cu(II).

binding sites in ZinT protein, corresponding to the N-terminal His-rich sequence (**L1** and **L2**) and to the 166–178 fragments (**L3** and **L4**). We calculated two competition plots to qualitatively evaluate the ligands affinity for Cu(II) and Zn(II) (Figure 6). The histidine-rich fragments **L1** and **L2** are better ligands for Zn(II) ion, confirming the general assumption that a higher number of histidine residues favours the metal complexation.[45-47] Indeed, according to the proposed speciation models, ZinT short fragments form stable 4N complexes with Zn(II) already at pH around 6. On the contrary, **L3** and **L4** contain only 3 imidazole groups and they can only coordinate the metal ion by means of a ($3N_{Im}$, O^-) binding mode. Therefore, the proposed coordination hypotheses are in good agreement with the competition plot trend, which also confirms a comparable stability among the studied systems below pH 6, i.e. where all the peptides display a 3N coordination.

In the case of copper ion (Figure 6b), once again the crowded cluster of histidines in **L1** and **L2** provides a higher number of anchoring sites to favour the first steps of complexation. On the contrary, in **L3** and **L4** the available binding sites are located at the peptide sequence opposite sides (Ac-DHXXXXXXXXHFH-NH_2), likely preventing an effective complexation. However, increasing the pH value the calculated competition plots designate the longer fragments as the most effective ligands. In order to explain this result, it can be useful to observe that, under alkaline conditions, backbone amides gradually substitute His residues as donor groups. As a consequence, the number of histidines in the peptide sequence contributes to a lesser extent to the complex stabilization, while the length of the peptide (clearly greater for **L3** and **L4**) could favour the wrap and protection of the metal binding site, thus increasing the complex stability.

ZinT complex stability: a comparison with other biologically relevant metal binding systems

The above results on the complex-formation behaviour of ZinT allow a comparison with some biologically relevant metal binding systems in order to shed light on its mechanism of action in the metal acquisition processes at the host/pathogen interface.

The metal complexation ability of ZinT can be compared with that of the antimicrobial peptide calcitermin (VAIALKAAHYHTHKE), which is present in human airways and is able to bind quite effectively Zn(II) and Cu(II) ions (Figure S27 ESI).[48] Calcitermin contains three alternated histidines (HXHXH), two lysines, one glutamic acid and the free amino- and carboxyl-termini. Furthermore, its antimicrobial activity is enhanced in the presence of Zn(II) and Cu(II) at acidic conditions,[48] representing a possible natural competitor and antagonist of ZinT in the host human organism. The competition plots of Figure S27 ESI show that, under acidic conditions, calcitermin binds both Zn(II) and Cu(II) ions with the highest affinity. At such pH values its coordination sphere is very similar to that of ZinT complexes, with a ($3N_{Im}$, O^-) binding mode; however, the alternated His-tag (HXHXH) is confirmed to be an extremely effective binding motif, even with respect to the four histidine sequence HXHHXH of **L1** and **L2**. On the other hand, in the case of Cu(II) ion, starting from physiological pH, the **L3** and **L4** fragments become more efficient ligands than calcitermin. Interestingly, previous studies show that antimicrobial activity of calcitermin is lost at physiological pH.[48] Thus, the present results can suggest that its antimicrobial way of action is related to the metal binding affinities of the competing systems. A slight different behaviour occurs, instead, in the case of Zn(II) ion, where calcitermin almost steadily maintains its efficacy as ligand throughout the explored pH range.

According to recent studies performed on *Se*ZinT,[14] the metal recruitment mechanism of this protein should involve the formation of a binary complex with ZnuA, the soluble periplasmic component of ZnuABC transporter. This interaction has not been fully elucidated, but the presence of both the proteins in their Zn(II)-bound form seems to be crucial. Moreover, the N-terminal histidine-rich loop of ZnuA has been proved to play a critical role,[14] and some evidence also suggests

that ZnuA may interact with other metal ions, including Cu(II).[49] In order to compare the Zn(II) and Cu(II) metal binding ability of the ZinT fragments with that of the two identified metal binding sites of ZnuA from *E. coli*[50] (Ac-^{115}MKSIHGDDDDHDHAEKSDEDHHHGDFNMHLW^{145}-NH_2 , corresponding to the N-terminal His-rich loop, and Ac-^{223}GHFTVNPEIQPGAQRLHE^{240}-NH_2, a secondary and less effective binding site), the two competition plots shown in Figure S28 ESI have been computed. The comparison shows that ZnuA His-rich loop located in the domain 115–145 is by far the most effective ligand for Zn(II) ion. This is not surprising and confirms that a higher number (seven in this case) of histidines in the sequence favours the Zn(II) complexation and stabilizes the system. On the other hand, Cu(II) complexes of ZnuA His-rich loop do not exhibit an improved metal affinity with respect to ZinT, unless at the most acidic pH values. Interestingly, from the chemical point of view, although both ZnuA and ZinT (**L1** and **L2**) systems, under acidic conditions, form macrochelated complexes with the same $3N_{Im}$ coordination, the smaller number of His residues in ZinT leads to the binding of N-amides at lower pH and therefore earlier with respect to ZnuA. The N-amides coordination induces an increased square-planar character and the possible formation of stable 5/6-membered-rings involving the imidazole and vicinal peptide amides. Above physiological conditions, as previous described, **L3** and **L4** peptides are able to form 4N complexes and exhibit the highest binding ability. Lastly, the two His-containing ZnuA fragment Ac-^{223}GHFTVNPEIQPGAQRLHE^{240}-NH_2 has been proved to be the less effective ligand.

The different results obtained for Zn(II) and Cu(II) complexes may explain the ZinT biological activity towards these metals. Although ZinT is able to bind both the ions and participate to Zn(II) recruitment, no evidence of its role in Cu(II) homeostasis has been found and indeed some studies exclude this function.[15] Moreover, the extremely high binding affinity of ZnuA His-rich loop towards Zn(II) is fully consistent with the putative mechanism of zinc transfer from ZinT to ZnuA *via* the formation of the protein binary system. Based on our results, such process cannot occur in the case of Cu(II), since the ZnuA fragments proved to be inadequate to catch the metal ion.

Conclusions

The thermodynamic and spectroscopic results obtained in the present work are consistent with previous biological studies conducted on ZinT. The metal binding site corresponding to the 166–178 amino acid sequence (*E. coli* **L3** = Ac-DHIIAPRKSSHFH-NH_2 and *S. enterica* **L4** = Ac-DHIIAPRKSAHFH-NH_2) is confirmed to be fundamental for metal coordination, particularly involving the three histidine (H167, H176, H178) and the aspartic acid (D166) residues. Furthermore, the spectroscopic near-UV CD structural characterization of **L3** and **L4** apo-peptides and of their Cu(II) and Zn(II) complexes does not highlight the formation of any particular α-helical or β-sheet structure and the typical band at around 200 nm confirms a flexible random coil conformation (Figures S29, S30 ESI).

However, the obtained thermodynamic equilibrium constants designate also the N-terminal histidine-rich fragment (^{24}HGHHXH^{29}) as a very effective metal binding domain. In fact, the results presented in this work reveal that **L1** = Ac-HGHHAH-NH_2 (*Ec*ZinT) and especially **L2** = Ac-HGHHAH-NH_2 (*Se*ZinT) exhibit the highest affinity for the Zn(II) ion all over the explored pH range. These fragments are also able to better stabilize Cu(II) complexes, but only under acidic conditions, which are, nonetheless, quite common during infections.

No remarkable differences between *E. coli* and *S. enterica* model systems have been observed. The coordination behaviour is similar for **L1** and **L2** as well as for **L3** and **L4**, respectively, although some minor differences occur under the most alkaline conditions. However, it is worth to underline that peptides from *Ec*ZinT show a higher tendency to stabilize Cu(II) complexes at neutral and alkaline pH, i.e. when backbone amides participate in Cu(II) coordination. This trend has been observed in many other systems and ascribed to a possible electronic effect of serine residues, capable of favouring the amidic proton displacement by the Cu(II) ion.[44, 45, 51]

The metal binding behaviour of ZinT fragments is fully consistent with the previously formulated hypotheses about the protein biological role. The high efficacy of HGHHXH in metal chelation is in line with the necessity to recover and stabilize as much micronutrients as possible from the medium, acting as a primary metal scavenger. Subsequently, its function may involve the delivery of the metal ion to ZinT canonical binding site (**L3** and **L4** fragments) for storage and/or transfer to other proteins (e.g. ZnuA). The His-rich loop may therefore represent the first, but temporary, stop station for the metal ion on its route to cellular import. Indeed, a relatively high metal binding affinity is crucial to ensure the acquisition process in an environment rich of competitive systems. It is therefore not surprising that the histidine-rich loop of *E. coli* ZnuA (Ac-MKSIHGDDDDHDHAEKSDEDHHHGDFNMHLW-NH_2) exhibits the strongest Zn(II) affinity in comparison with the ligands studied in this work. ZinT is supposed to directly interact with ZnuA, forming a binary complex in the presence of zinc ions and likely transferring the metal to the partner protein through the His-rich loop of ZnuA. This process can be successfully achieved only if the ZnuA metal binding site has a higher affinity for Zn(II) than ZinT, and this is the case highlighted by our results. Surprisingly, Cu(II) complexes behave in a different way. In this case, the ZnuA His-rich loop shows a less effective metal binding ability, resulting in a higher stability of Cu(II) complexes with ZinT. Although further investigations are necessarily required, our thermodynamic results reflect previous observations according to which ZinT should not participate in Cu(II) homeostasis.

The results of the present study shed a new light on the way of action of the ZinT/ZnuABC transport system. The elucidation of the metal–protein interaction based on thermodynamics and coordination chemistry is an indispensable starting point to develop metal-based drugs. Taking advantage from the Zn(II) chelating properties, a possible antimicrobial strategy can be related to the design of a Zn(II) chelating system that can ultimately interact with both ZinT and ZnuA forming an irreversible (ternary) complex ZinT–(Zn(II)-pharmacophore)–

ZnuA. This may starve the pathogen by preventing the transfer of the metal ion to the ZnuB component and putting out of play both the proteins in charge of metal recruitment.

Conflicts of interest

There are no conflicts to declare.

Acknowledgements

Financial supports by the National Science Centre (UMO-2017/26/A/ST5/00363 and UMO-2017/26/A/ST5/00364), the University of Ferrara (FAR 2019) and the Erasmus+ Programme are gratefully acknowledged. This paper is based upon work from COST Action CA18202, NECTAR – Network for Equilibria and Chemical Thermodynamics Advanced Research, supported by COST (European Cooperation in Science and Technology).

Notes and references

1. J. P. Zackular, R. J. Knippel, C. A. Lopez, W. N. Beavers, C. N. Maxwell, W. J. Chazin and E. P. Skaar, *mSphere*, 2020, **5**, e00061-00020.
2. P. Chandrangsu, C. Rensing and J. D. Helmann, *Nat. Rev. Microbiol.*, 2017, **15**, 338-350.
3. R. E. W. Hancock and H.-G. Sahl, *Nat. Biotechnol.*, 2006, **24**, 1551.
4. P. Kumar, V. Dalal, N. Sharma, S. Kokane, D. K. Ghosh, P. Kumar and A. K. Sharma, *Metallomics*, 2020, **12**, 280-289.
5. Z. Ma, F. E. Jacobsen and D. P. Giedroc, *Chem. Rev.*, 2009, **109**, 4644-4681.
6. K. P. Grim, J. N. Radin, P. K. Párraga Solórzano, J. R. Morey, K. A. Frye, K. Ganio, S. L. Neville, C. A. McDevitt and T. E. Kehl-Fie, *J. Bacteriol.*, 2020, JB.00014-00020.
7. S. Gillet, E. Lawarée and J.-Y. Matroule, in *Microbial Diversity in the Genomic Era*, eds. S. Das and H. R. Dash, Academic Press, 2019, ch. 23, pp. 409-426.
8. P. Petrarca, S. Ammendola, P. Pasquali and A. Battistoni, *J. Bacteriol.*, 2010, **192**, 1553-1564.
9. S. I. Patzer and K. Hantke, *Mol. Microbiol.*, 1998, **28**, 1199-1210.
10. Z. R. Lonergan and E. P. Skaar, *Trends Biochem. Sci*, 2019, **44**, 1041-1056.
11. S. Campoy, M. Jara, N. Busquets, A. M. Pérez De Rozas, I. Badiola and J. Barbé, *Infect. Immun.*, 2002, **70**, 4721-4725.
12. R. Gabbianelli, R. Scotti, S. Ammendola, P. Petrarca, L. Nicolini and A. Battistoni, *BMC Microbiol.*, 2011, **11**, 36-36.
13. S. Ammendola, P. Pasquali, C. Pistoia, P. Petrucci, P. Petrarca, G. Rotilio and A. Battistoni, *Infect. Immun.*, 2007, **75**, 5867-5876.
14. A. Ilari, F. Alaleona, G. Tria, P. Petrarca, A. Battistoni, C. Zamparelli, D. Verzili, M. Falconi and E. Chiancone, *Biochim. Biophys. Acta*, 2014, **1840**, 535-544.
15. H. G. Colaço, P. E. Santo, P. M. Matias, T. M. Bandeiras and J. B. Vicente, *Metallomics*, 2016, **8**, 327-336.
16. T. Stojnev, J. Harichová, P. Ferianc and T. Nyström, *Curr. Microbiol.*, 2007, **55**, 99-104.
17. C. J. Kershaw, N. L. Brown and J. L. Hobman, *Biochem. Biophys. Res. Commun.*, 2007, **364**, 66-71.
18. G. David, K. Blondeau, M. Schiltz, S. Penel and A. Lewit-Bentley, *J. Biol. Chem.*, 2003, **278**, 43728-43735.
19. J. Chen, L. Wang, F. Shang, Y. Dong, N.-C. Ha, K. H. Nam, C. Quan and Y. Xu, *Biochem. Biophys. Res. Commun.*, 2018, **500**, 139-144.
20. The UniProt Consortium, *Nucleic Acids Res.*, 2018, **47**, D506-D515.
21. J. A. Lemire, J. J. Harrison and R. J. Turner, *Nat. Rev. Microbiol.*, 2013, **11**, 371-384.
22. K. S. Chaturvedi and J. P. Henderson, *Front. Cell. Infect. Microbiol.*, 2014, **4**, 1-12.
23. J. B. Cross, J. S. Duca, J. J. Kaminski and V. S. Madison, *J. Am. Chem. Soc.*, 2002, **124**, 11004-11007.
24. N. Fushimi, C. n. E. Ee, T. Nakajima and E. Ichishima, *J. Biol. Chem.*, 1999, **274**, 24195-24201.
25. N. Giebeler and P. Zigrino, *Toxins (Basel)*, 2016, **8**, 122-122.
26. S. Damo and T. E. Kehl-Fie, in *Antimicrobial Peptides: Role in Human Health and Disease*, eds. J. Harder and J.-M. Schröder, Springer International Publishing, Cham, 2016, pp. 89-100.
27. S. R. Hennigar and J. P. McClung, *Am. J. Lifestyle Med.*, 2016, **10**, 170-173.
28. P. Gans and B. O'Sullivan, *Talanta*, 2000, **51**, 33-37.
29. G. Gran, *Acta Chem. Scand.*, 1950, **4**, 559-577.
30. P. Gans, A. Sabatini and A. Vacca, *Talanta*, 1996, **43**, 1739-1753.
31. G. Arena, R. Cali, E. Rizzarelli and S. Sammartano, *Therm. Acta*, 1976, **16**, 315-321.
32. C. F. Baes and R. E. Mesmer, *The hydrolysis of cations*, John Wiley & Sons, Ltd., New York, 1976.
33. L. Alderighi, P. Gans, A. Ienco, D. Peters, A. Sabatini and A. Vacca, *Coord. Chem. Rev.*, 1999, **184**, 311-318.
34. H. Sigel and R. B. Martin, *Chem. Rev.*, 1982, **82**, 385-426.
35. L. D. Pettit and H. K. J. Powell, *The IUPAC Stability Constants Database*, Royal Society of Chemistry, London, 1992-2000.
36. J. Makowska, K. Bagińska, A. Liwo, L. Chmurzyński and H. A. Scheraga, *Biopolymers*, 2008, **90**, 724-732.
37. J. Makowska, A. Liwo, L. Chmurzyński and H. A. Scheraga, *J. Solution Chem.*, 2012, **41**, 1738-1746.
38. B. Noszál and E. Osztás, *Int. J. Pept. Protein Res.*, 1989, **33**, 162-166.
39. J. Peisach and W. E. Blumberg, *Arch. Biochem. Biophys.*, 1974, **165**, 691-708.
40. K. Ősz, K. Várnagy, H. Süli-Vargha, A. Csámpay, D. Sanna, G. Micera and I. Sóvágó, *J. Inorg. Biochem.*, 2004, **98**, 24-32.
41. P. Deschamps, P. P. Kulkarni, M. Gautam-Basak and B. Sarkar, *Coord. Chem. Rev.*, 2005, **249**, 895-909.
42. L. Casella, M. E. Silver and J. A. Ibers, *Inorg. Chem.*, 1984, **23**, 1409-1418.
43. M. Sola, A. Lledos, M. Duran and J. Bertran, *Inorg. Chem.*, 1991, **30**, 2523-2527.
44. D. Bellotti, C. Tocchio, R. Guerrini, M. Rowińska-Żyrek and M. Remelli, *Metallomics*, 2019, **11**, 1988-1998.
45. D. Bellotti, D. Łoboda, M. Rowińska-Żyrek and M. Remelli, *New J. Chem.*, 2018, **42**, 8123-8130.
46. M. Remelli, M. Peana, S. Medici, L. G. Delogu and M. A. Zoroddu, *Dalton Trans.*, 2013, **42**, 5964-5974.
47. H. Kozlowski, M. Łuczkowski and M. Remelli, *Dalton Trans.*, 2010, **39**, 6371-6385.

View Article Online
DOI: 10.1039/D0DT01626H

48. D. Bellotti, M. Toniolo, D. Dudek, A. Mikołajczyk, R. Guerrini, A. Matera-Witkiewicz, M. Remelli and M. Rowińska-Żyrek, *Dalton Trans.*, 2019, **48**, 13740-13752.
49. L. A. Yatsunyk, J. A. Easton, L. R. Kim, S. A. Sugarbaker, B. Bennett, R. M. Breece, I. I. Vorontsov, D. L. Tierney, M. W. Crowder and A. C. Rosenzweig, *J. Biol. Inorg. Chem.*, 2008, **13**, 271-288.
50. A. Hecel, A. Kola, D. Valensin, H. Kozlowski and M. Rowinska-Zyrek, *Inorg. Chem.*, 2020, **59**, 1947-1958.
51. P. Mlynarz, D. Valensin, K. Kociolek, J. Zabrocki, J. Olejnik and H. Kozlowski, *New J. Chem.*, 2002, **26**, 264-268.

View Article Online
DOI: 10.1039/D0DT01626H

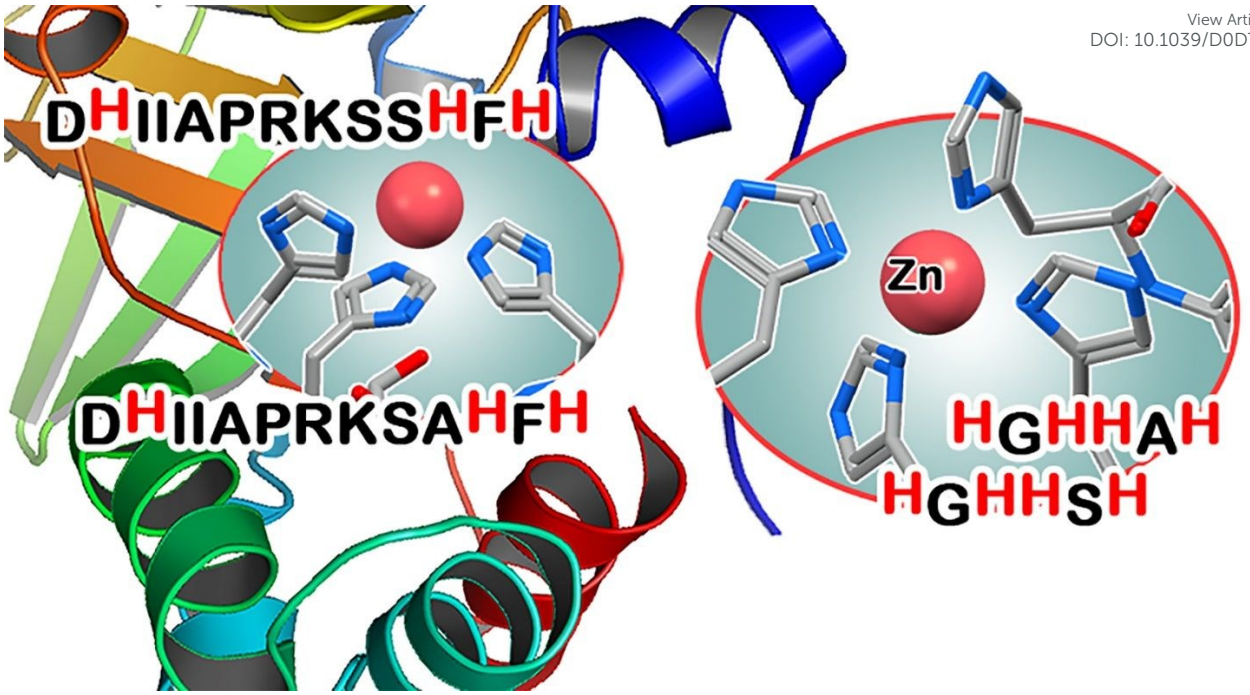

The characterization of Zn(II) and Cu(II) complexes with the periplasmic protein ZinT suggests that the N-terminal histidine-rich loop has a role as primary metal scavenger and that ZinT can possibly transfer a Zn(II) ion to ZnuA.